

Unraveling the Quantum Mpemba Effect on Markovian Open Quantum Systems

Rodrigo F. Saliba¹ and Raphael C. Drumond²

¹Departamento de Física, Universidade Federal de Minas Gerais,

²Departamento de Matemática, Universidade Federal de Minas Gerais

(Dated: December 16, 2025)

In recent years, the quantum Mpemba effect (QME) — which occurs when an out of equilibrium system reaches equilibrium faster than another which is closer to equilibrium — has attracted significant attention from the scientific community as an intriguing and counterintuitive phenomenon. It generalizes its classical counterpart, extending the concept beyond temperature equilibration. This paper approaches the QME for markovian open quantum systems in different perspectives. Firstly, we propose a physical mechanism based on decoherence free subspaces. Secondly, we show that an exponential growth in the decay rate towards equilibrium which scales with system size can be obtained, leading to an extreme version of the phenomenon on markovian open quantum systems. Thirdly, we study the strong Mpemba effect through the unravelings of Davies Maps, revealing subtleties in the figures of merit which are chosen for obtaining the QME. Lastly, we propose a microscopic model for better understanding of bath dynamics in this context.

I. INTRODUCTION

Throughout history, several cultures, philosophers, and scientists have written about the phenomenon in which an initially hot system cools down faster than an initially colder one. Some of the historical figures who noticed and described this effect include Aristotle [1], Francis Bacon [2], and René Descartes [3]. The first systematic studies of the phenomenon were conducted by Mpemba, Osborne, and Kell [4, 5], and the effect has since been referred to as the *Mpemba effect*.

Numerous studies have explored the Mpemba effect in different kinds of systems since Mpemba and Osborne's initial work [6–8], although the existence of the effect as originally described by Mpemba remains a topic of debate in the literature [9, 10].

Nevertheless, descriptions of quantum analogues of this classical effect are now well established. These Mpemba-like effects occur when an initially out-of-equilibrium state reaches equilibrium faster than a state closer to equilibrium. This phenomenon, known as the *quantum Mpemba effect* (QME), has been observed in both closed and open quantum systems [11].

In the context of Markovian open quantum systems, recent works have shown that for systems governed by specific types of equations of motion, it is always possible to find a unitary transformation of an initial state that leads to a state with higher energy, which in turn exhibits an exponentially faster relaxation toward equilibrium—given an arbitrary initial state with coherences in the energy eigenbasis [12, 13].

Although mathematically rigorous frameworks for obtaining such states have been developed, the physical mechanisms underlying the QME in Markovian open quantum systems are still poorly understood [14, 15]. Here, we explore one possible mechanism and its consequences. Moreover, we study the previously explored method for obtaining states exhibiting the strong quantum Mpemba effect through the lens of quantum trajectories, aiming for a deeper understanding of the phe-

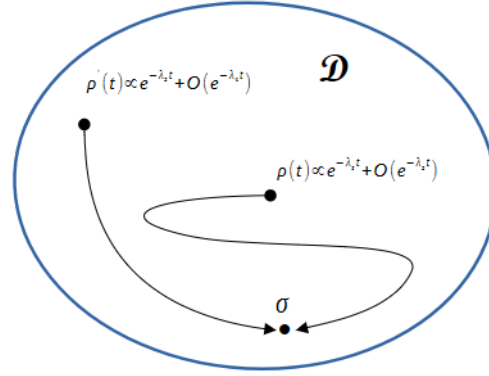


FIG. 1: Illustrative picture of the quantum Mpemba effect.

nomenon in this context.

The paper is organized as follows: Section II reviews the mathematical description of the strong quantum Mpemba effect. Section III presents one possible physical mechanism for the QME. Section IV discusses the strong quantum Mpemba effect through the lens of quantum trajectories. Section V studies system–bath interactions with the help of a microscopic model based on Gaussian systems.

II. MPEMBA EFFECT IN MARKOVIAN OPEN QUANTUM SYSTEMS

Markovian open quantum system dynamics obey an equation of motion that can, in general, be written in Lindblad form [16–18]:

$$\frac{d\rho}{dt} = \mathcal{L}[\rho] = -i[H, \rho] + \sum_k \lambda_k \left(L_k \rho L_k^\dagger - \frac{1}{2} \{ L_k^\dagger L_k, \rho \} \right). \quad (1)$$

Here, \mathcal{L} is the Liouvillian superoperator, λ_k are the dissipation rates, $[\cdot, \cdot]$ and $\{\cdot, \cdot\}$ denote the commutator and anticommutator, respectively, and L_k are usually called *jump operators*. The form of the L_k depends on the specific problem being considered [11, 19, 20].

A special example of such equations is given by the class of dynamics known as *Davies maps* [21]. An important property of these equations is that their steady state is the thermal (Gibbs) state,

$$\rho_{ss} = \frac{e^{-\beta H}}{\text{Tr}[e^{-\beta H}]} \quad (2)$$

This allows the observation of the quantum Mpemba effect through thermalization, in close analogy with its classical counterpart.

Mathematically, the state of the system at an arbitrary time can be expanded in terms of the Liouvillian eigenoperators as

$$\rho(t) = e^{\mathcal{L}t} \rho(0) = \sigma + \sum_{k=2}^D \text{Tr}[\mathbf{l}_k \rho(0)] \mathbf{r}_k e^{\lambda_k t}, \quad (3)$$

where D is the dimension of the Hamiltonian, σ is the thermal state (the right eigenoperator of \mathcal{L} associated with the zero eigenvalue), and \mathbf{l}_k and \mathbf{r}_k are the left and right eigenoperators of \mathcal{L} associated with the eigenvalue λ_k , respectively [22].

Given an initial state $\rho(0)$, if the eigenvalues are ordered in ascending order according to the absolute value of their real parts, i.e.,

$$0 = \lambda_1 \leq |\text{Re}(\lambda_2)| \leq |\text{Re}(\lambda_3)| \leq \dots,$$

it can be shown that an exponential speed-up of the system's thermalization may be achieved if there exists a unitary operator U acting on \mathbf{l}_2 such that

$$\text{Tr}[\mathbf{l}_2 U \rho(0) U^\dagger] = 0$$

[13], where it is assumed that λ_2 is real (see Fig. 1).

If λ_2 is complex, the main contributions to the evolution of the density matrix are given by

$$\rho(t) \propto \sigma + e^{\text{Re}(\lambda_2)t} \left(\text{Tr}[\mathbf{l}_2 \rho(0)] \mathbf{r}_2 e^{i \text{Im}(\lambda_2)t} + \text{Tr}[\mathbf{l}_2^\dagger \rho(0)] \mathbf{r}_2^\dagger e^{-i \text{Im}(\lambda_2)t} \right). \quad (4)$$

Thus, the unitary operator must satisfy both

$$\text{Tr}[\mathbf{l}_2 U \rho(0) U^\dagger] = 0 \quad \text{and} \quad \text{Tr}[\mathbf{l}_2^\dagger U \rho(0) U^\dagger] = 0.$$

A procedure can then be developed to obtain the corresponding unitary for an initial state $\rho(0)$ with coherences in the energy eigenbasis. This transformation consists of bringing the state into diagonal form in that basis [12].

There are many quantities that may be used as metrics for measuring the distance between two states [11]. Here,

we focus on the non-equilibrium free energy, following the approach of Moroder *et al.* [12]:

$$F_{\text{neq}} = \langle H \rangle - TS_{\text{vn}}, \quad (5)$$

where H is the system Hamiltonian, T is the temperature, and $S_{\text{vn}} = -\text{Tr}[\rho \ln \rho]$ is the von Neumann entropy.

This figure of merit is monotonic in time and allows one to observe the QME in Davies maps. The QME occurs if there exists a time τ such that $F_{\text{neq}}(\rho'(t)) < F_{\text{neq}}(\rho(t))$ for $t > \tau$, where the initial state ρ' has a higher non-equilibrium free energy than ρ .

Another quantity used in this work as a measure of how fast the state approaches equilibrium is the trace distance [11]:

$$d_{\text{Tr}}(\rho, \sigma) = \frac{1}{2} \text{Tr}[\sqrt{A^\dagger A}], \quad (6)$$

where $A = \rho - \sigma$. The same qualitative behavior as for F_{neq} is expected for this metric, with the exception of the regime $T = 0$ (see Section IV).

As an example, consider a single qubit coupled to a bosonic bath at temperature T , with Hamiltonian $H = \frac{1}{2}\omega\sigma_z$. The system's state may be expressed in terms of the Pauli matrices as

$$\rho = \frac{1}{2} [\mathbb{I} + r_1 \sigma_x + r_2 \sigma_y + r_3 \sigma_z], \quad (7)$$

where $\mathbf{R} = (r_1, r_2, r_3)$ is the Bloch vector.

The Davies map for this setup is given by

$$\frac{d\rho}{dt} = -i[H, \rho] + \gamma_- (\bar{N} + 1) \mathcal{D}(\sigma_-) + \gamma_+ (\bar{N}) \mathcal{D}(\sigma_+), \quad (8)$$

where \bar{N} is the Bose-Einstein distribution and $\mathcal{D}(L) = L\rho L^\dagger - \{L^\dagger L, \rho\}$.

The results for the evolution of F_{neq} and d_{Tr} for ρ and ρ' , obtained using the procedure outlined above, are shown in Fig. 2.

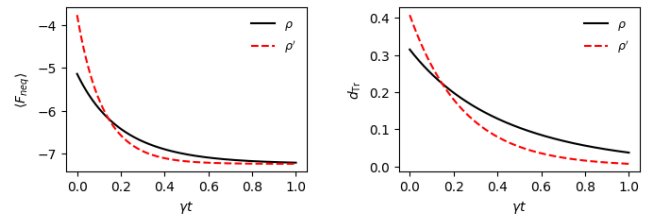


FIG. 2: Evolution of the non-equilibrium free energy (a) and trace distance (b) for the states ρ and $\rho' = U\rho U^\dagger$. The state ρ' is observed to exhibit lower values of F_{neq} and d_{Tr} than ρ after a certain elapsed time,

characterizing the quantum Mpemba effect in this system. The parameters used are $\omega = 5$, $\gamma_+ = \gamma_- = 1$, and $T = 10\gamma_+$. The initial state ρ is defined by the Bloch vector $\mathbf{R} = (0.52807291, 0.21585042, 0.02214326)$.

III. COLLECTIVE DECAY AND DECOHERENCE-FREE SUBSPACES

Consider a system of non-interacting spin systems with Hamiltonian:

$$H = J_z \sum_i \frac{1}{2} \sigma_i^z, \quad (9)$$

where J_z is the energy gap between states $|\uparrow_i\rangle$ and $|\downarrow_i\rangle$. The system is assumed to undergo both collective and local (thermal) dissipation, in such a way that its dynamics is governed by the master equation:

$$\begin{aligned} \frac{d\rho}{dt} = & -i[H, \rho] + \Gamma \mathcal{D}(L_c) \\ & + \sum_k [\mu(1 + \bar{N}) \mathcal{D}(S_k^-) + \mu \bar{N} \mathcal{D}(S_k^+)], \end{aligned} \quad (10)$$

where $L_c = \sum_i S_i^- = S_c^-$ is the collective decay Lindblad operator, and Γ and μ represent the dissipation strengths associated with the collective and thermal decays, respectively. This model is closely related to superradiance [23–26], where the collective interference of emission pathways leads to enhanced, cooperative decay.

We choose the initial states of the system to be the all-up state $|\uparrow\rangle = |\uparrow\uparrow\cdots\uparrow\rangle$ (which corresponds, in the context of superradiance, to the state where all atoms are in the excited state $|e\cdots e\rangle$) and a non-trivial state taken from a decoherence-free subspace.

In order to understand our choice of states, consider a pair of two-level systems whose only source of dissipation is collective decay and assume that $\mu = 0$ in the model. In this case, the initial states are chosen to be the triplet state $|\psi\rangle = |\uparrow\uparrow\rangle$, which has maximum energy, and the singlet state $|\phi\rangle = \frac{1}{\sqrt{2}}(|\uparrow\downarrow\rangle - |\downarrow\uparrow\rangle)$, which has zero initial energy.

The result of the evolution under the master equation (10) for both states is shown in Fig. 3a. The singlet state's non-equilibrium free energy is trapped at $F_{\text{neq}} = 0$. When local dissipation ($\mu \neq 0$, but with $\mu < \Gamma$) is considered, the singlet state then decays to the lower energy state, but at the slower rate μ , while the triplet state still decays at the faster rate Γ . This is shown in Fig. 3b.

Now, based on our discussion so far, a necessary condition for the QME is that different initial states decay at different rates. The effect occurs when we can vary initial states in such a way as to simultaneously increase both their distance from equilibrium and their decay rate.

As suggested by the example in Eq. (10), a simple mechanism to achieve this is to exploit dissipators with decoherence-free subspaces (DFS). Namely, assume a system governed by a Lindblad equation with two dissipators, \mathcal{D}_{dfs} and \mathcal{D}_{per} , having distinct rates Γ and μ , respectively, where $\Gamma \gg \mu$. If \mathcal{D}_{dfs} possesses a DFS, but the combined dissipator $\mathcal{D}_{\text{dfs}} + \mathcal{D}_{\text{per}}$ has a unique steady state, then states inside the DFS decay slowly (at rate μ), while states outside it decay rapidly (at rate Γ). The

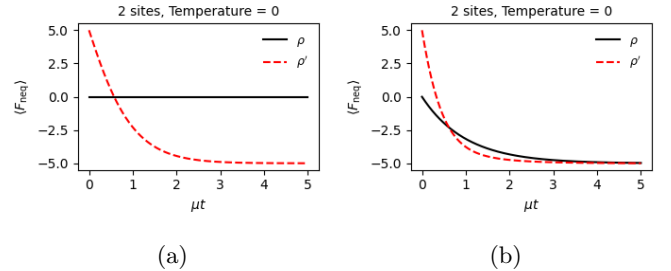


FIG. 3: (a) Non-equilibrium free energy for triplet (red line) and singlet (black line) for evolution under collective decay. The result shows that the singlet state is trapped in its initial state if no local dissipator is used ($\mu = 0$) and $J_z = 5$. (b) Same parameters, but with $\mu = 1$.

QME will take place provided there exists a state outside the DFS that is farther from equilibrium than a state inside it.

Coming back to the model described by Eq. (10), we explore its behavior for a larger number of spins. To this end, we used states from a decoherence-free subspace that take the following form:

$$|\psi\rangle = \frac{1}{\sqrt{L}} \sum_{i=1}^L (-1)^i |\downarrow_1\rangle \cdots |\downarrow_{i-1}\rangle |\uparrow_i\rangle |\downarrow_{i+1}\rangle \cdots |\downarrow_L\rangle. \quad (11)$$

As a starting point, we evaluated the robustness of this mechanism to temperature changes. The results (Fig. 4) show that the quantum Mpemba effect still occurs at temperatures greater than zero. Moreover, it can be seen that the quantum Mpemba effect holds even for very high temperatures, as shown in Fig. 4c.

Next, the behavior of the model regarding the size of the system was probed. Here we see that the effect still holds, as shown in Fig. 5. These results provide evidence that one can exploit decoherence-free subspaces as a mechanism to arrive at the quantum Mpemba effect for both few- and many-body systems.

A. Extreme Quantum Mpemba Effect

Another consequence of our model with collective decay can be more easily seen when, instead of using the decoherence-free subspace, we consider a state for which the above Hamiltonian leads to a zero expected value for the energy. Since the states treated here are pure, the initial non-equilibrium free energy reduces to $F_{\text{neq}} = \langle H \rangle = 0$. For this model, the subspace with this property consists of states with zero total magnetization, i.e., spin-up on half of the sites and spin-down on the other half, e.g.,

$$|\psi\rangle = |\downarrow_1\rangle \otimes \cdots \otimes |\downarrow_{L/2}\rangle \otimes |\uparrow_{(L/2+1)}\rangle \otimes \cdots \otimes |\uparrow_L\rangle. \quad (12)$$

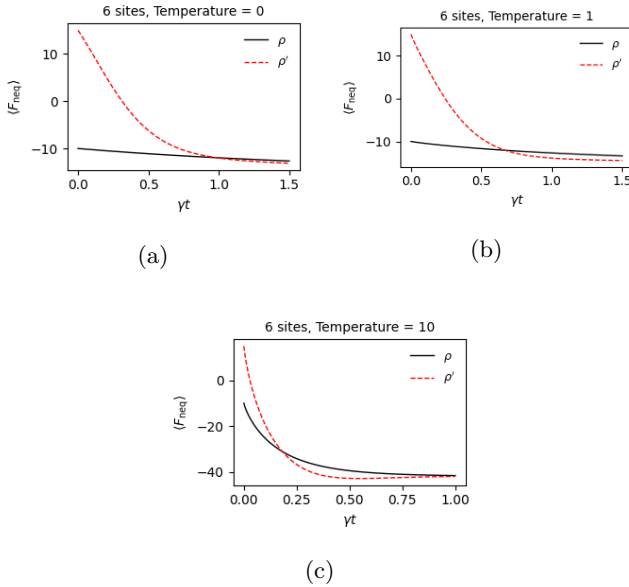


FIG. 4: Non-equilibrium free energy for the all-up state (red line) and decoherence-free subspace state (black line) for evolution under collective dissipation at 3 different temperatures, where $T = 0\Gamma, 1\Gamma$, and 10Γ for (a), (b), and (c), respectively. Here, the parameters used were $J_z = 5$, $\Gamma = 1$, and $\mu = 1$.

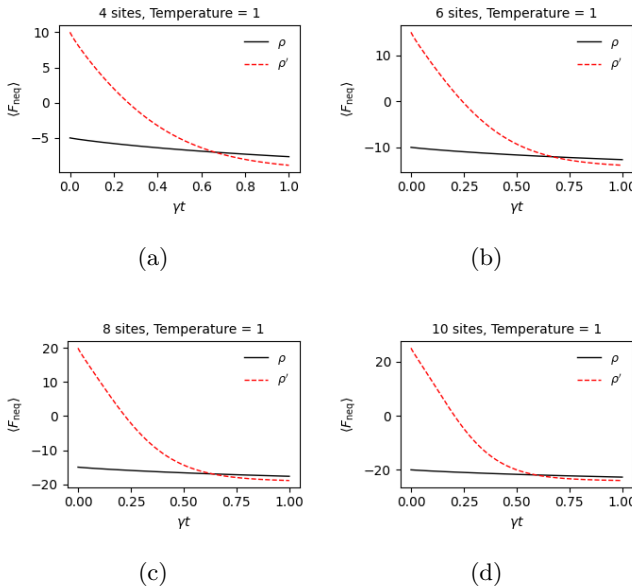


FIG. 5: Non-equilibrium free energy for the all-up state (red line) and decoherence-free subspace state (black line) for evolution under collective dissipation at temperature $T = 1\Gamma$. Here, the parameters used were $J_z = 5$, $\Gamma = 1$, and $\mu = 0.5$.

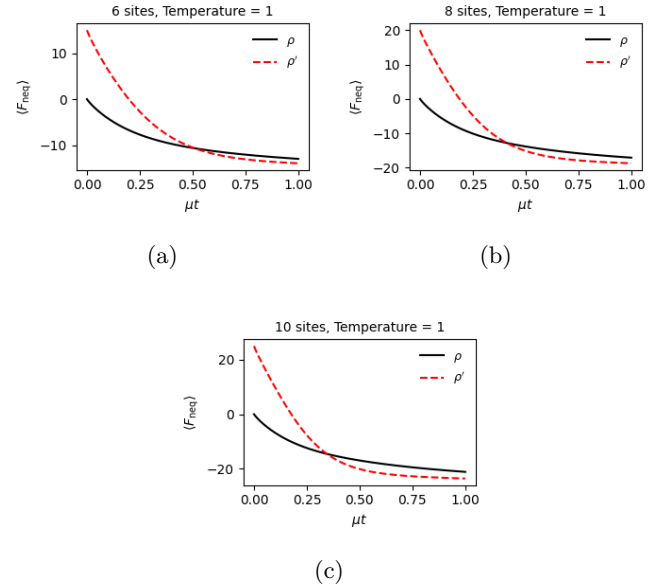


FIG. 6: Non-equilibrium free energy for the all-up state (red line) and decoherence-free subspace state (black line) for evolution under collective dissipation at temperature $T = 1\Gamma$. Here, the parameters used were $J_z = 5$, $\Gamma = 1$, and $\mu = 1$.

L	t_{c1}
4	0.70
6	0.50
8	0.41
10	0.34

TABLE I: Approximate time of crossing (t_{c1}) for the results of F_{neq} in Fig. 6 as the number of sites of the system L grows. Here, t_{c1} indicates the time evolved for temperature set to $T = 1\Gamma$.

From this perspective, the all-up state is seen to decay faster as the system size grows, showing that an extreme version of the quantum Mpemba effect, where the relaxation towards equilibrium of ρ' can be made as fast as one desires, can be obtained by increasing the system size. This feature is shown for systems up to 10 sites in Fig. 6. Here, the time of crossing between the non-equilibrium free energy of both states becomes shorter as the system size grows (see Table I).

In order to show that the result is truly dependent on the system size, we solve the master equation for the simplified model

$$\frac{d\rho}{dt} = -i[H, \rho] + \gamma \left[S_c^- \rho S_c^+ - \frac{1}{2} \{ S_c^+ S_c^-, \rho \} \right] \quad (13)$$

where the Hamiltonian may be written as $H = J_z S_c^z$ and is identical to the one in equation (9).

In this case, one can use the concept of coherent spin states, where spin states are associated with number states in quantum optics [27]. Consider a collection of

S spins and define the fully polarized down state as $|0\rangle$,

$$S_c^z |0\rangle = -S |0\rangle. \quad (14)$$

The state with p spin excitations can then be written as

$$(S_c^+)^p |0\rangle = \sqrt{\frac{p!(2S)!}{(2S-p)!}} |p\rangle, \quad (15)$$

where $0 \leq p \leq 2S$, and $|p\rangle$ denotes the normalized Dicke state with p excitations.

A spin coherent state can be defined as

$$|\chi\rangle = \frac{1}{(1+|\chi|^2)^S} \exp(\chi S_c^+) |0\rangle. \quad (16)$$

In the large-spin limit $S \rightarrow \infty$, the Holstein–Primakoff transform yields the approximate mapping [27]

$$S_c^- \rightarrow \sqrt{2S} a, \quad (17)$$

$$S_c^+ \rightarrow \sqrt{2S} a^\dagger, \quad (18)$$

$$S_c^z \rightarrow a^\dagger a - S, \quad (19)$$

$$\chi \rightarrow \frac{\alpha}{\sqrt{2S}}, \quad (20)$$

under which the spin coherent state becomes the bosonic coherent state

$$|\alpha\rangle = \exp\left(-\frac{1}{2}|\alpha|^2\right) \exp(\alpha a^\dagger) |0\rangle. \quad (21)$$

In this limit, the collective-spin Hamiltonian $H = J_z S_c^z$ reduces to the harmonic-oscillator Hamiltonian $H \simeq J_z a^\dagger a$ (up to a constant), and the master equation for the collective decay channel becomes

$$\frac{d\rho}{dt} = -iJ_z \left[a^\dagger a - \frac{N}{2}, \rho \right] + N\gamma \left[a\rho a^\dagger - \frac{1}{2} \{ a^\dagger a, \rho \} \right], \quad (22)$$

where $N = 2S$ is the total number of atoms and $N\gamma$ is the effective collective decay rate in the harmonic-oscillator description.

Assuming the system starts at a coherent state $\rho(0) = |\alpha\rangle\langle\alpha|$, where $|\alpha(t)\rangle = e^{\alpha a^\dagger - \alpha^* a} |0\rangle$, we get (see appendix A):

$$\dot{\alpha} = (-iJ_z - \frac{N}{2}\gamma)\alpha \implies \alpha(t) = e^{-iJ_z - \frac{N}{2}\gamma t} \alpha(0), \quad (23)$$

$$\dot{\alpha}^* = (iJ_z - \frac{N}{2}\gamma)\alpha^* \implies \alpha^*(t) = e^{iJ_z - \frac{N}{2}\gamma t} \alpha^*(0), \quad (24)$$

which shows that the decay rate increases as system size grows. Note that the coherent states in these approximations cover the all spins-up state when $|\alpha| \rightarrow \infty$, but do not approximate the singlet states that we have shown to decay slowly.

IV. UNRAVELINGS AND PROBABILITY DYNAMICS FOR DAVIES MAPS

In order to probe the mechanisms behind the strong Mpemba effect as outlined in Section II, we first consider the model of a single qubit coupled to a thermal bath at zero temperature. The system Hamiltonian is given by

$$H = \frac{1}{2}\sigma^z, \quad (25)$$

and the full Lindblad equation reads

$$\frac{d\rho}{dt} = -i[H, \rho] + \mu\mathcal{D}(\sigma^-). \quad (26)$$

Using the procedure given by Moroder *et al.* [12], we obtained the states that exhibit the QME. However, F_{neq} does not capture the effect for these states at zero temperature, since the crossing of the curves depends on how the von Neumann entropy varies. On the other hand, the trace distance still shows that ρ' reaches the equilibrium state faster (see Fig. 7). Thus, the trace distance allows us to study the system in its simplest form. To that end, we focus on the unravelings of the master equation for the two states.

From the numerical results for single trajectories, we observe that after the first jump the states are both in the steady state (Fig. 8a), which, for this example, is the ground state. For pure states, ρ' is always given by the excited state (the highest-energy eigenvector of this Hamiltonian). Assuming ρ is the density matrix for a general pure state $|\psi\rangle(t) = \alpha(t)|0\rangle + \beta(t)|1\rangle$, the probabilities P_1 and P'_1 for a jump operator to act upon the states in a time interval δt are

$$P'_1 = \mu\delta t, \quad P_1 = \mu|\beta(t)|^2\delta t. \quad (27)$$

Since $|\beta(t)|^2 \leq 1$, the probability of the first jump to happen for ρ' is always higher than for $\rho \neq \rho'$. On the other hand, there is a probability $|\alpha(0)|^2$ for $|\psi\rangle$ to reach the ground state without a quantum jump. Assuming this is the case, the evolution of the state amplitudes follows [28]:

$$\begin{aligned} \alpha(t) &= \alpha(0) \left[|\alpha(0)|^2 + |\beta(0)|^2 e^{-\mu t} \right]^{-\frac{1}{2}}, \\ \beta(t) &= \beta(0) e^{-\frac{\mu t}{2}} \left[|\alpha(0)|^2 + |\beta(0)|^2 e^{-\mu t} \right]^{-\frac{1}{2}}. \end{aligned} \quad (28)$$

Thus, even if the quantum jump does not occur for $|\psi\rangle$, it will reach the ground state with an exponential rate $e^{-\mu t/2}$. This makes the survival probability, i.e., the probability that no jump occurs up to time t , behave as

$$\begin{aligned} P'_s(t) &= e^{-\mu t}, \\ P_s(t) &= |\alpha(0)|^2 + |\beta(0)|^2 e^{-\mu t}. \end{aligned} \quad (29)$$

Thus,

$$\frac{dP_s}{dt} = |\beta(0)|^2 \frac{dP'_s}{dt},$$

and the survival probability decays more slowly for $|\psi\rangle$. As a consequence, the survival probability for $|\psi\rangle$ is higher than that of $|1\rangle$ for all $\mu t > 0$. Along with Eq. (27), this guarantees that the averaged trajectories of the excited state reach the ground state faster than those for $|\psi\rangle$.

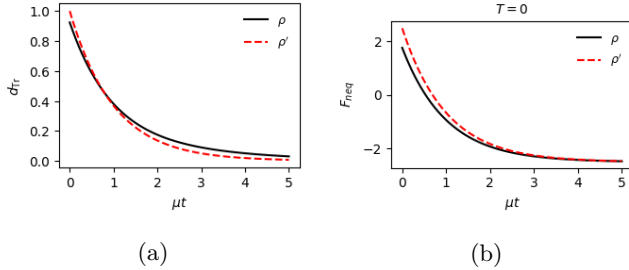


FIG. 7: Trace distance (a) and non-equilibrium free energy (b) for pure ρ and ρ' . Here $T = 0$, $\mu = 1$, and the initial state is determined by the Bloch vector $\mathbf{R} = (0.0025964, -0.70710201, 0.70710678)$.

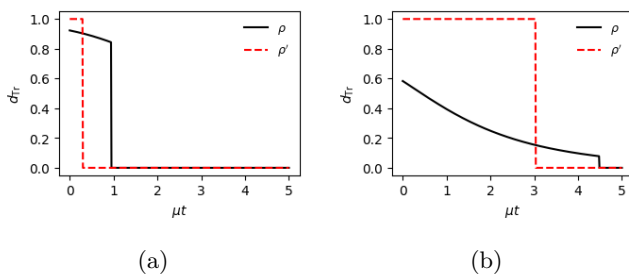


FIG. 8: Sample trajectory of the conditional trace distance for the states $\rho = \frac{1}{2} [\mathbb{I} + r_1\sigma^x + r_2\sigma^y + r_3\sigma^z]$ and $\rho' = |1\rangle\langle 1|$. (a) shows the typical behavior for two pure states, where $\mathbf{R} = (0.0025964, -0.70710201, 0.70710678)$, and (b) shows the comparison with a mixed state, where $\mathbf{R} = (0.52807291, 0.21585042, 0.02214326)$.

Comparing ρ' and a general mixed state

$$\rho = \begin{pmatrix} |\beta|^2 & c \\ c^* & |\alpha|^2 \end{pmatrix}, \quad (30)$$

one still obtains the effect (Fig. 8b) with the same probabilities as in Eq. (27). This indicates that, if we take ρ' to be the excited state, the phenomenon is not caused by intrinsically quantum-mechanical effects, since the coherences play no role in the jump probabilities of this state.

In the opposite regime, $T \gg 0$, the same idea governs the behavior of the two states. However, since another jump operator now plays a role in the dynamics, the probabilities for the first jump to occur in a time interval δt change to

$$P'_1 = \mu(\bar{N} + 1)\delta t, \quad P_1 = \mu(\bar{N} + |\beta(t)|^2)\delta t, \quad (31)$$

and ρ' will, on average, undergo more jumps before the first jump of ρ .

Thus, the averaged ρ' over trajectories becomes more mixed faster and reaches thermalization more quickly.

Returning to F_{neq} , Fig. 9 corroborates our description of the jump-probability dynamics underlying the quantum Mpemba effect. In these circumstances, the survival probabilities of ρ' and ρ behave as (Fig. 9a)

$$\begin{aligned} P'_s(t) &= \exp[-\mu(\bar{N} + 1)t], \\ P_s(t) &= |\alpha(0)|^2 \exp[-\mu\bar{N}t] + |\beta(0)|^2 \exp[-\mu(\bar{N} + 1)t]. \end{aligned} \quad (32)$$

Here one finds that

$$\frac{dP_s}{dt} = \left(\frac{\bar{N} + |\beta(0)|^2}{\bar{N} + 1} \right) \frac{dP'_s}{dt},$$

and, as in the zero-temperature case, for $|\beta(0)| < 1$ the survival probability for ρ changes more slowly than for ρ' .

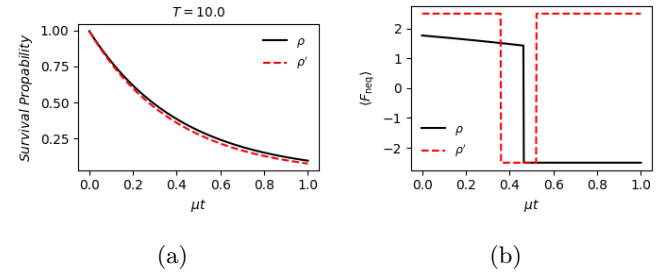


FIG. 9: (a) Survival probability evolution for ρ and ρ' , where both states are pure. (b) Sample trajectory for the evolution of the non-equilibrium free energy for both states. The parameters are the same as in Fig. 10.

The Bloch vector for ρ is
 $\mathbf{R} = (0.0025964, -0.70710201, 0.70710678)$.

For mixed states, it becomes interesting to look into the entropy averaged over trajectories, $\bar{S}_{\text{vn}}(\rho(t))$. The von Neumann entropy is a highly non-linear quantity, and the average over unravelings generally leads to behavior that differs from the entropy of the averaged state, $\bar{S}_{\text{vn}}(\rho(t))$ (For an example of this method, see [29].). This allows the extraction of additional information from the system.

As seen in Fig. 10a, the averaged entropy term in F_{neq} takes longer to reach its steady state for ρ' . Since the von Neumann entropy is a measure of purity, we have that ρ' , on average, takes longer to become pure. Looking at single trajectories (see Fig. 10b), one sees that one of the main factors contributing to the behavior of the averaged entropy is that the entropy of the state ρ' increases much faster than that of ρ before the first jump, which is attributed to ρ' being diagonal in the energy eigenbasis [12]. The trajectories also show that, after the first jump, both states remain pure for the rest of the evolution.

The survival probabilities have a similar behavior as for pure states (Fig. 10c), since the initial state ρ' has higher excited-state population by construction [12]. Here, coherences play an important role, since we can write the eigenvalues of the general density matrix in Eq. (30) as

$$\begin{aligned}\lambda_{\pm}(t) &= \frac{1 \pm \sqrt{1 - 4 \det \rho(t)}}{2} \\ &= \frac{1 \pm \sqrt{1 - 4(\beta(t)(1 - \beta(t)) - |c(t)|^2)}}{2},\end{aligned}\quad (33)$$

and the speed-up of

$$S_{vn} = -(\lambda_+ \ln \lambda_+ + \lambda_- \ln \lambda_-)$$

is larger if $|c'(0)| \ll |c(0)|$, where c' and c are the coherences of ρ' and ρ , respectively.

This becomes clear when we consider the explicit forms of $\beta(t)$ and $|c(t)|$:

$$\begin{aligned}\beta(t) &= \beta_{\text{eq}} + (\beta(0) - \beta_{\text{eq}}) \exp\left[-\frac{\mu}{2}(\bar{N} + 1)t\right], \\ |c(t)|^2 &= |c(0)|^2 \exp(-\mu t),\end{aligned}\quad (34)$$

where β_{eq} is the excited-state population of the equilibrium state.

Thus, as the temperature grows, the decay rate of $|c(t)|^2$ becomes slower than that of $\beta(t)$, which reduces the change in entropy. Figure 11 shows the comparison of the results for state evolution with the same ρ as in Fig. 10. Here, we explicitly used the states

$$\rho'_1 = \begin{pmatrix} 0.7 & 0.1 \\ 0.1 & 0.3 \end{pmatrix}, \quad \rho'_2 = \begin{pmatrix} 0.7 & 0.3 \\ 0.3 & 0.3 \end{pmatrix}. \quad (35)$$

V. BOSONIC GAUSSIAN SYSTEMS AND A MICROSCOPIC MODEL

In order to understand the role of coherences in the system–bath interaction, we propose a microscopic model in which we keep track of the bath state. In this context, we study a Gaussian bosonic system consisting of a single mode of an optical cavity (a single harmonic oscillator [30]) coupled to a bath of harmonic oscillators. This is done using the covariance-matrix formalism, where the initial states of the system are chosen to be Gaussian and the states of each oscillator in the bath are thermal. The system is completely characterized by its covariance matrix σ and first moments \mathbf{r} [30, 31], defined as

$$\mathbf{r} = \langle \mathbf{R} \rangle, \quad (36)$$

$$\sigma_{ij} = \frac{1}{2} \langle R_i R_j + R_j R_i \rangle - \langle R_i \rangle \langle R_j \rangle, \quad (37)$$

where \mathbf{R} is a $2N$ -dimensional vector defined in terms of the quadrature operators,

$$\mathbf{R} = (q_1, p_1, \dots, q_N, p_N), \quad (38)$$

$$q_i = \frac{1}{\sqrt{2}}(a_i + a_i^\dagger), \quad p_i = \frac{1}{i\sqrt{2}}(a_i - a_i^\dagger). \quad (39)$$

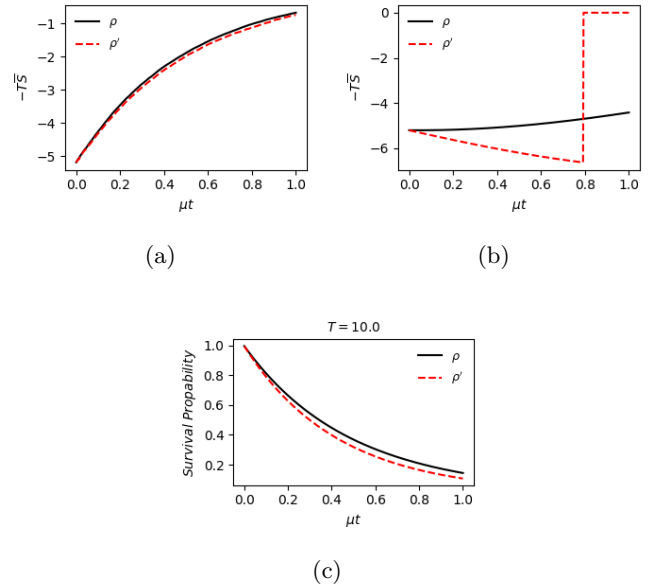


FIG. 10: (a) Average over trajectories of $-TS$. Here we see a faster increase of the entropy for ρ' , which is one of the factors leading the averaged state to remain mixed longer than ρ . (b) Sample trajectory of the conditional non-equilibrium free energy for the states $\rho = \frac{1}{2}[\mathbb{I} + r_1\sigma^x + r_2\sigma^y + r_3\sigma^z]$ and ρ' . (c) Survival probability evolution for both states. Here we used $J_z = 5$, $\mu = 1$, $T = 10\mu$, and the Bloch vector was $\mathbf{R} = (0.52807291, 0.21585042, 0.02214326)$.

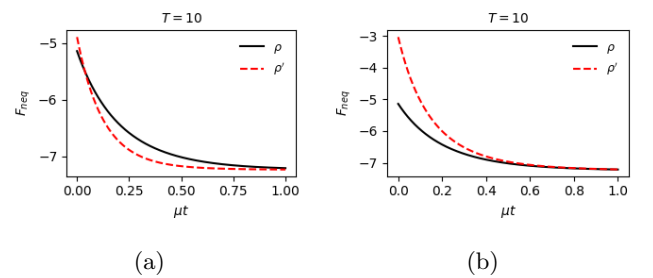


FIG. 11: Comparison between states with the same populations but different coherences. The states ρ and ρ' are given by Eq. (30) and Eq. (35), respectively. (a) shows the results for the lower-coherence state in Eq. (35), and (b) shows the results for the higher-coherence state. Here we used $J_z = 5$, $\mu = 1$, $T = 10\mu$, and the Bloch vector was $\mathbf{R} = (0.52807291, 0.21585042, 0.02214326)$.

The dynamics for a $N = 2001$ mode system was then simulated. The first moments and covariance matrix obey the equations of motion [30, 31]

$$\frac{d\mathbf{r}}{dt} = -W\mathbf{r}, \quad (40)$$

$$\frac{d\sigma}{dt} = -(W\sigma + \sigma W^\dagger), \quad (41)$$

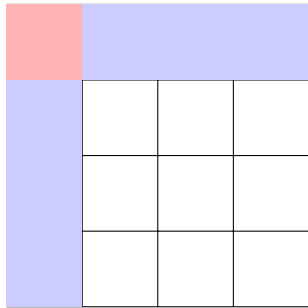


FIG. 12: Illustrative diagram of the covariance matrix and the blocks used to quantify the correlation strength between the system and the environment.

where $W = -\Omega \mathbf{H}$, with \mathbf{H} written in terms of \mathbf{R} , and Ω is the N -mode symplectic form

$$\Omega = \bigoplus_{k=1}^N \omega, \quad \omega = \begin{pmatrix} 0 & 1 \\ -1 & 0 \end{pmatrix}. \quad (42)$$

The first mode is taken as the system, and the remaining modes constitute the bath (initially in a thermal state).

The correlations between the system and bath modes are quantified through the Frobenius norm of the corresponding submatrices, which provides information about the correlation between the first and the n th mode (see Fig. 12). In order to obtain the quantum Mpemba effect, we select a coherent state and a squeezed vacuum state whose initial non-equilibrium free energy is higher than that of the former. The squeezed vacuum state tends to suppress odd excitations [32] and has fewer coherences in the energy eigenbasis. This allows for an earlier crossing of the curves.

In Fig. 13b we show the total correlation dynamics, defined as the sum of the Frobenius norms of all sub-blocks of σ :

$$\text{total correlation} = \sum_i (\|\sigma_{0,i}\|_F + \|\sigma_{i,0}\|_F). \quad (43)$$

The results show a greater correlation build-up for the squeezed vacuum state, which supports the idea that, in this case, the smaller number of coherences in the energy eigenbasis leads to faster interactions with the bath frequencies, which in turn leads the squeezed vacuum state to thermalize faster than the coherent state. To show that this build-up of correlations is indeed different across bath modes for the chosen states, we show in Figs. 13c and 13d the correlation evolution of each bath mode with the system.

Thus, from the viewpoint of quantum trajectories, one arrives at the notion that the strong QME is caused by an interplay of jump probabilities between eigenstates, which are generally larger for states with higher excited-state populations. Coherences are of great importance for mixed states, since large coherences inhibit the faster

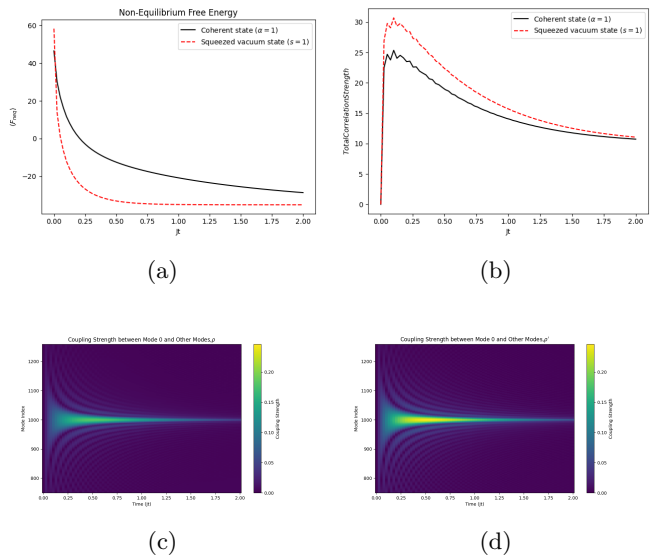


FIG. 13: (a) Non-equilibrium free energy for the states $\rho = D(\alpha) |0\rangle\langle 0| D^\dagger(\alpha)$ and $\rho' = S(s) |0\rangle\langle 0| S^\dagger(s)$ (coherent and squeezed vacuum states). (b) Total correlation strength between the system and the bath. (c)–(d) 2D plots showing the dynamics of the correlation strength between the system and each bath mode. Here we used $\alpha = 1$ and $s = 1$.

relaxation of the state with higher excited-state population. This is further supported by the system–bath correlation build-up of states with different amounts of coherence in the energy eigenbasis, which shows that the state with fewer coherences (and higher initial F_{neq}) builds up larger correlations with the bath during its dynamics.

VI. CONCLUSION

We have shown that one possible mechanism for obtaining the quantum Mpemba effect in Markovian open quantum systems is to exploit decoherence-free subspaces. This method has proven robust to changes in temperature and system size, and it opens new possibilities for utilizing the effect in many areas, such as quantum optics [25, 33] and ultracold gases [23]. As a consequence of this mechanism, an extreme version of the quantum Mpemba effect can be achieved, characterized by an exponential speed-up toward the equilibrium state with system size. This has been shown both numerically and analytically (Section III and Appendix A).

The strong quantum Mpemba effect has also been explored at the level of trajectories, revealing an interesting dynamics of jump probabilities which, when averaged, yields the effect. Here, the most striking result is the dependence of the strong QME on the excited-state population and its inhibition by coherences. The role of coherences was further tested with a proposed microscopic model in which we kept track of the system–bath dynam-

ics in a bosonic system, showing that states with fewer coherences build up larger correlations with the bath and, as a consequence, thermalize faster.

ACKNOWLEDGMENTS

This study was financed in part by the Coordenação de Aperfeiçoamento de Pessoal de Nível Superior – Brasil (CAPES) – Finance Code 001.

Appendix A: Analytical Description of the Decay at Zero Temperature

In order to solve this problem, we consider the system to start in a coherent state $\rho(0) = |\alpha\rangle\langle\alpha|$, assuming α to be time dependent:

$$|\alpha(t)\rangle = D(\alpha(t))|0\rangle = e^{\alpha a^\dagger - \alpha^* a}|0\rangle. \quad (\text{A1})$$

Using the identity $e^{A+B} = e^A e^B e^{\frac{1}{2}[A,B]}$, we can write

$$D(\alpha(t)) = e^{-\frac{|\alpha|^2}{2}} e^{\alpha a^\dagger} e^{-\alpha^* a}. \quad (\text{A2})$$

The following identities can then be obtained:

$$\frac{\partial D(\alpha)}{\partial \alpha} = \left(a^\dagger - \frac{1}{2}\alpha^* \right) D(\alpha), \quad (\text{A3})$$

$$\frac{\partial D(\alpha)}{\partial \alpha^*} = - \left(a - \frac{1}{2}\alpha \right) D(\alpha), \quad (\text{A4})$$

and thus, taking the time derivative of $|\alpha\rangle$ yields

$$\begin{aligned} \frac{d}{dt} |\alpha\rangle &= \frac{\partial D(\alpha)}{\partial \alpha} \dot{\alpha}|0\rangle + \frac{\partial D(\alpha)}{\partial \alpha^*} \dot{\alpha}^*|0\rangle \\ &= \left[\dot{\alpha}(a^\dagger - \frac{1}{2}\alpha^*) - \dot{\alpha}^*(a - \frac{1}{2}\alpha) \right] |\alpha\rangle. \end{aligned} \quad (\text{A5})$$

The left-hand side of Eq. (22) for a coherent state therefore reads

$$\begin{aligned} \frac{d\rho}{dt} &= \left[\dot{\alpha}(a^\dagger - \frac{1}{2}\alpha^*) - \dot{\alpha}^*(a - \frac{1}{2}\alpha) \right] \rho \\ &+ \rho \left[\dot{\alpha}(a^\dagger - \frac{1}{2}\alpha^*) - \dot{\alpha}^*(a - \frac{1}{2}\alpha) \right]^\dagger, \end{aligned} \quad (\text{A6})$$

Using the defining property of a coherent state, namely that it is an eigenstate of the annihilation operator,

$a|\alpha\rangle = \alpha|\alpha\rangle$, the right-hand side of Eq. (22) becomes

$$\begin{aligned} \frac{d\rho}{dt} &= -iJ_z(\alpha a^\dagger|\alpha\rangle\langle\alpha| - |\alpha\rangle\langle\alpha|a^*a) \\ &+ 2S\gamma(|\alpha|^2|\alpha\rangle\langle\alpha| - \frac{1}{2}\alpha a^\dagger|\alpha\rangle\langle\alpha| - \frac{1}{2}|\alpha\rangle\langle\alpha|a^*a). \end{aligned} \quad (\text{A7})$$

Now, we note that

$$\begin{aligned} D^\dagger(\alpha)a^\dagger D(\alpha) &= a^\dagger + [a^\dagger, \alpha a^\dagger - \alpha^* a] + \dots \\ &= a^\dagger + \alpha^*, \end{aligned} \quad (\text{A8})$$

where we used the Baker–Campbell–Hausdorff (BCH) formula[34] and the fact that

$$[[a^\dagger, \alpha a^\dagger - \alpha^* a], \alpha a^\dagger - \alpha^* a] = [\alpha^*, \alpha a^\dagger - \alpha^* a] = 0, \quad (\text{A9})$$

since α^* is a complex number.

Using $D^\dagger(\alpha)D(\alpha) = \mathbb{I}$, we can express the action of a^\dagger on $|\alpha\rangle$ as

$$\begin{aligned} a^\dagger|\alpha\rangle &= a^\dagger D(\alpha)|0\rangle = D(\alpha)(D^\dagger(\alpha)a^\dagger D(\alpha))|0\rangle \\ &= D(\alpha)(a^\dagger + \alpha^*)|0\rangle = \alpha^*|\alpha\rangle + |1_\alpha\rangle, \end{aligned} \quad (\text{A10})$$

where $|1_\alpha\rangle = D(\alpha)a^\dagger|0\rangle$.

Substituting Eq. (A10) into Eqs. (A6) and (A7), we obtain

$$\begin{aligned} \dot{\alpha}|1_\alpha\rangle\langle\alpha| + \dot{\alpha}^*|\alpha\rangle\langle 1_\alpha| &= -iJ_z(\alpha|\alpha\rangle\langle 1_\alpha| - \alpha^*|1_\alpha\rangle\langle\alpha|) \\ &- S\gamma(\alpha|1_\alpha\rangle\langle\alpha| + \alpha^*|\alpha\rangle\langle 1_\alpha|), \end{aligned} \quad (\text{A11})$$

which leads directly to Eqs. (23) and (24).

[1] H. D. P. Lee *et al.*, *Meteorologica*, Vol. 397 (Cambridge, Harvard, 1952).

[2] F. Bacon, *Novum organum* (Clarendon press, 1878).

[3] R. Descartes, *Discourse on the method: And, meditations on first philosophy* (Yale University Press, 1996).

[4] E. B. Mpemba and D. G. Osborne, Cool?, *Physics Education* **4**, 172 (1969).

[5] G. S. Kell, The freezing of hot and cold water, *American Journal of Physics* **37**, 564 (1969).

[6] P. Chaddah, S. Dash, K. Kumar, and A. Banerjee, Overtaking while approaching equilibrium, arXiv preprint arXiv:1011.3598 (2010).

[7] C. Hu, J. Li, S. Huang, H. Li, C. Luo, J. Chen, S. Jiang, and L. An, Conformation directed mpemba effect on polylactide crystallization, *Crystal Growth & Design* **18**, 5757 (2018).

[8] P. A. Greaney, G. Lani, G. Cicero, and J. C. Grossman, Mpemba-like behavior in carbon nanotube resonators, *Metallurgical and Materials Transactions A* **42**, 3907 (2011).

[9] H. C. Burridge and P. F. Linden, Questioning the mpemba effect: Hot water does not cool more quickly than cold, *Scientific Reports* **6**, 37665 (2016).

[10] J. Bechhoefer, A. Kumar, and R. Chétrite, A fresh understanding of the mpemba effect, *Nature Reviews Physics* **3**, 534 (2021).

[11] F. Ares, P. Calabrese, and S. Murciano, The quantum mpemba effects, *Nature Reviews Physics* **1** (2025).

[12] M. Moroder, O. Culhane, K. Zawadzki, and J. Goold, Thermodynamics of the quantum mpemba effect, *Physical Review Letters* **133**, 140404 (2024).

[13] F. Carollo, A. Lasanta, and I. Lesanovsky, Exponentially accelerated approach to stationarity in markovian open quantum systems through the mpemba effect, *Physical Review Letters* **127**, 060401 (2021).

[14] S. Longhi, Quantum mpemba effect from initial system-reservoir entanglement, *APL Quantum* **2** (2025).

[15] S. Longhi, Quantum mpemba effect from non-normal dynamics, *Entropy* **27**, 581 (2025).

[16] H.-P. Breuer and F. Petruccione, *The theory of open*

quantum systems (OUP Oxford, 2002).

- [17] G. Lindblad, On the generators of quantum dynamical semigroups, *Communications in mathematical physics* **48**, 119 (1976).
- [18] V. Gorini, A. Kossakowski, and E. C. G. Sudarshan, Completely positive dynamical semigroups of n-level systems, *Journal of Mathematical Physics* **17**, 821 (1976).
- [19] G. T. Landi, M. J. Kewming, M. T. Mitchison, and P. P. Potts, Current fluctuations in open quantum systems: Bridging the gap between quantum continuous measurements and full counting statistics, *PRX Quantum* **5**, 020201 (2024).
- [20] A. J. Daley, Quantum trajectories and open many-body quantum systems, *Advances in Physics* **63**, 77 (2014).
- [21] E. B. Davies, Markovian master equations, *Communications in mathematical Physics* **39**, 91 (1974).
- [22] $\mathcal{L}[\mathbf{r}_k] = \lambda_k \mathbf{r}_k$ and $\mathcal{L}^\dagger[\mathbf{l}_k] = \lambda_k \mathbf{l}_k$.
- [23] I. Bloch, J. Dalibard, and W. Zwerger, Many-body physics with ultracold gases, *Reviews of modern physics* **80**, 885 (2008).
- [24] R. H. Dicke, Coherence in spontaneous radiation processes, *Physical Review* **93**, 99 (1954).
- [25] M. Gross and S. Haroche, Superradiance: An essay on the theory of collective spontaneous emission, *Physics Reports* **93**, 301 (1982).
- [26] F. Damanet, A. J. Daley, and J. Keeling, Atom-only descriptions of the driven-dissipative dicke model, *Physical Review A* **99**, 033845 (2019).
- [27] J. M. Radcliffe, Some properties of coherent spin states, *Journal of Physics A: General Physics* **4**, 313 (1971).
- [28] K. Mølmer, Y. Castin, and J. Dalibard, Monte carlo wave-function method in quantum optics, *Journal of the Optical Society of America B* **10**, 524 (1993).
- [29] X. Cao, A. Tilloy, and A. De Luca, Entanglement in a fermion chain under continuous monitoring, *SciPost Physics* **7**, 024 (2019).
- [30] G. Adesso, S. Ragy, and A. R. Lee, Continuous variable quantum information: Gaussian states and beyond, *Open Systems & Information Dynamics* **21**, 1440001 (2014).
- [31] G. T. Landi, D. Poletti, and G. Schaller, Nonequilibrium boundary-driven quantum systems: Models, methods, and properties, *Reviews of Modern Physics* **94**, 045006 (2022).
- [32] C. C. Gerry and P. L. Knight, *Introductory quantum optics* (Cambridge university press, 2023).
- [33] M. O. Scully and A. A. Svidzinsky, The super of superradiance, *Science* **325**, 1510 (2009).
- [34] $e^{-A} B e^A = B + [B, A] + \frac{1}{2!} [[B, A], A] + \dots$